Pinpointing gap minima in Ba(Fe$_{0.94}$Co$_{0.06}$)$_2$As$_2$ via band-structure calculations and electronic Raman scattering

I. I. Mazin,[1] T. P. Devereaux,[2] J. G. Analytis,[2] Jiun-Haw Chu,[2] I. R. Fisher,[2] B. Muschler,[3] and R. Hackl[3]

[1]*Code 6393, Naval Research Laboratory, Washington, DC 20375, USA*

[2]*Stanford Institute for Materials and Energy Science, SLAC National Accelerator Laboratory and Department of Applied Physics, Stanford University, Stanford, California 94305, USA*

[3]*Walther Meissner Institut, Bayerische Akademie der Wissenschaften, 85748 Garching, Germany*

A detailed knowledge of the gap structure for the Fe-pnictide superconductors is still rather rudimentary with several conflicting reports of either nodes, deep gap minima, or fully isotropic gaps on the Fermi-surface sheets, both in the k_x-k_y plane and along the c axis. In this Rapid Communication, we present considerations for electronic Raman scattering which can help clarify the gap structure and topology using different light-scattering geometries. Using density-functional calculations for the Raman vertices, it is shown that the location of the gap minima may occur on loops stretching over a portion of the c axis in Ba(Fe$_{0.94}$Co$_{0.06}$)$_2$As$_2$.

Since the discovery of high-temperature superconductivity in the iron pnictides, identifying the structure of the superconducting order parameter has remained a tantalizing and elusive problem. Knowledge of the momentum dependence is a major step toward identifying the interactions that drive the superconductivity. A variety of experimental techniques probing the low-energy properties of the pnictides in the superconducting state have given contradictory information on the angular dependence of the superconducting gap around the Fermi surfaces (FS). Angle-resolved photoemission on NdFeAsO$_{0.9}$F$_{0.1}$,[1] K-doped,[2] and Co-doped[3] BaFe$_2$As$_2$ have identified rather isotropic superconducting gaps on both the hole and electron pockets in the Brillouin zone (BZ). On the other hand, transport and thermodynamic measurements, which do not have angular resolution, have indicated the presence of nodes in some materials and small but finite gaps in others.[4] Recently, angle-resolved thermal conductivity in BaFe$_2$(As,P)$_2$ have indicated large gap variations around the Fermi surface with gap nodes or deep minima located at 45° with respect to the principal BZ axes.[5]

Electronic Raman-scattering experiments indicated very small gaps located on the electron Fermi surfaces in Ba(Fe$_{0.94}$Co$_{0.06}$)$_2$As$_2$.[6] However, due to the relative insensitivity of the Raman vertices to momentum in the canonical tight-binding (TB) scheme the location of the nodes could not be determined uniquely. The situations is additionally obscured by the fact that the electronic structure of the 122 materials is inherently more three-dimensional (3D) than that of the 1111 pnictides and simplified two-dimensional (2D) tight-binding models can be rather misleading.[7] Moreover, the crystallographic symmetry of the 122 structure is body-centered tetragonal (bct), $I4/mmm$, therefore folding down the Fermi surfaces from the one-Fe Brillouin zone to the two-Fe zone is less trivial than in the 1111 structure. Namely, while in the 1111 structure the electronic pockets at the X point and Y point in the unfolded zone are related by a simple $\pi/2$ rotation, so that after folding they form e-pockets with the full fourfold symmetry, in the 122 structure the symmetry operation connecting the two unfolded pockets is the same rotation plus a shift along k_z by π/c. Thus for all k_z but $k_z = \pi/2c$ the folded FS cuts have only a twofold symmetry.

Incidentally, for the same reason the standard method of constructing a TB Hamiltonian by transforming the Bloch functions into the Wannier functions leads to a TB model that attempts to describe the outer barrel as a single band in the unfolded BZ (Ref. 7) while in reality it is formed by anticrossing the X and the Y pockets. In other words, such TB models feature unphysically and artificially large interlayer hoppings (some interlayer hoppings in Ref. 7 appear to be more than 50% of the nearest-neighbor in-plane hopping), while in reality the scale of the k_z dispersion is set by the hybridization gaps, and by the difference in size (but not orientation) between the upper and the lower panel in Fig. 4 of Ref. 7.

For this reason, in the 122 systems extracting quantitative information from the experiment using an infolded 2D tight-binding model becomes questionable and working in a folded 3D TB model is not much simpler than straight off first-principles calculations. Therefore, in order to gain more accurate information about the location of gap minima on the Fermi surface we have performed all-electron band-structure calculations, as described in Ref. 8 and numerically computed the relevant Raman vertices. We have confirmed the result obtained qualitatively by Muschler *et al.*[6] that two of the three principal Raman symmetries, A_{1g} and B_{2g} (all notations in the crystallographic unit cell), probe, respectively, an average gap and the gap on the electron Fermi surface, and that for the third symmetry, B_{1g}, the matrix elements are mostly small on all the FSs. However, we found that on the outer electronic FS there exist "hot spots" where this matrix element is sizeable, a fact that could not be seen in unfolded TB calculations. The importance of the folded 3D two-Fe unit cell therefore allows us to show that we cannot only distinguish between the hole and the electron FSs in terms of the gap minima but can also place them at or near these hot spots (which appear near the [110] direction).

First, we discuss the so-called "effective-mass approximation" as applied to this compound. The inelastic light (Raman) scattering cross section in the limit of small momentum transfers is given in terms of correlation functions of an effective charge density,[9] $\tilde{\rho} = \Sigma_{n,\mathbf{k},\sigma}\gamma_n(\mathbf{k},\omega_i,\omega_s)c^\dagger_{n,\mathbf{k},\sigma}c_{n,\mathbf{k},\sigma}$, where $c^\dagger_{n,\mathbf{k},\sigma}$ ($c_{n,\mathbf{k},\sigma}$) creates (removes) an electron with mo-

mentum $\mathbf{k}$ and spin σ from band n. In principle, γ depends both on light-scattering polarization geometries $\mathbf{e}^{i(s)}$ and the frequencies of incoming (scattered) light $\omega^{i(s)}$. In the limit where $\omega^{i(s)}$ are much smaller than any relevant interband transition frequency, the scattering amplitude simplifies into the well-known effective-mass tensor

$$\gamma_n(\mathbf{k}, \omega^{i,s} \to 0) = \sum_{\alpha,\beta=x,y,z} e_\alpha^i \frac{\partial^2 \varepsilon_n(\mathbf{k})}{\partial k_\alpha \, \partial k_\beta} e_\beta^s. \quad (1)$$

For tetragonal materials, three different scattering geometries can be classified according to the point-group transformation properties. These are given as

$$A_{1g}: \gamma_n(\mathbf{k}) = [\partial^2 \varepsilon_n(\mathbf{k})/\partial k_x^2 + \partial^2 \varepsilon_n(\mathbf{k})/\partial k_y^2]/2,$$
$$B_{1g}: \gamma_n(\mathbf{k}) = [\partial^2 \varepsilon_n(\mathbf{k})/\partial k_x^2 - \partial^2 \varepsilon_n(\mathbf{k})/\partial k_y^2]/2,$$
$$B_{2g}: \gamma_n(\mathbf{k}) = \partial^2 \varepsilon_n(\mathbf{k})/\partial k_x \, \partial k_y. \quad (2)$$

Thus the curvature of the bands and the light-scattering polarization orientations determine which carriers are involved in light scattering in different bands and regions of the BZ. While not having the definitive angular resolution as photoemission to probe single-particle properties, Raman scattering can selectively project effective charge-density fluctuations in different regions of the BZ, uniquely providing k-projected dynamical two-particle properties.

In most systems, such as the cuprates and pnictides, incident light energies are typically high enough to directly excite interband charge transfer and thus the effective-mass approximation may be not valid for these systems. When this happens, strong resonance effects occur and the intensity of the electronic Raman scattering varies greatly with the incident photon energy, as, for instance, in some cuprates.[10] In Fig. 1 we present Raman data on a pnictide superconductor for three different excitation lines. The lack of change of the spectra for the different excitation lines demonstrate that off-resonance conditions for the scattering amplitude apply. Therefore we assume that the effective-mass approach holds for the pnictides and examine the full band and momentum dependence of the scattering amplitudes as a way of pinpointing the gap extrema structure.

In the superconducting state, the Raman response for B_{1g} and B_{2g} symmetries is given as a weighted average of the Tsuneto-Maki function λ_n over the FS for each band n,[11] $\chi_{\gamma,\gamma}(\Omega) = \Sigma_{n,\mathbf{k}} \gamma_n^2(\mathbf{k}) \lambda_n(\mathbf{k},\Omega)$, with the Raman vertices γ given in Eq. (2). The Tsuneto function is

$$\lambda_n(\mathbf{k},\Omega) = \tanh \frac{E_n(\mathbf{k})}{2k_B T} \frac{4|\Delta_n(\mathbf{k})|^2/E_n(\mathbf{k})}{4E_n^2(\mathbf{k}) - (\hbar\Omega + i\delta)^2}, \quad (3)$$

where $\Delta_n(\mathbf{k})$ is the superconducting gap in band n, having quasiparticle energy dispersion $\varepsilon_n(\mathbf{k})$, and $E_n^2(\mathbf{k}) = \varepsilon_n^2(\mathbf{k}) + \Delta_n^2(\mathbf{k})$. Enforcing particle number conservation, one gets

$$\chi(\Omega) = \chi_{\gamma,\gamma}(\Omega) - \chi_{\gamma,1}(\Omega)\chi_{1,\gamma}(\Omega)/\chi_{1,1}(\Omega) \quad (4)$$

with $\chi_{\gamma,1}(\Omega) = \chi_{1,\gamma}(\Omega) = \Sigma_{n,\mathbf{k}} \gamma_n(\mathbf{k}) \lambda_n(\mathbf{k},\Omega)$ and $\chi_{1,1}(\Omega) = \Sigma_{n,\mathbf{k}} \lambda_n(\mathbf{k},\Omega)$. Therefore, while for both B_{1g} and B_{2g} each contribution to the Raman vertex can be separated into contributions from single bands, the A_{1g} contributions mix mass
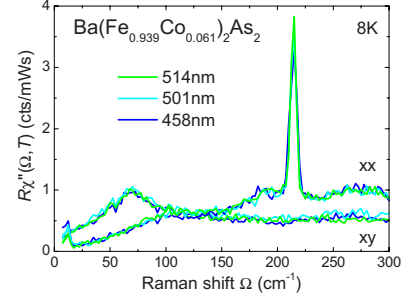

FIG. 1. (Color online) Raman response (Bose factor removed) for xx and xy polarizations for three different excitation lines as indicated. Apart from correcting for the instrumental response, the overall intensity is as measured and has not been shifted. To within the experimental error there is no dependence on the excitation energy demonstrating that resonance effects can be neglected.

fluctuations in each band and between bands.

In Ref. 6, the interplay of the energy gap and the symmetry dependence of the Raman vertices was considered, where it was argued that B_{2g} polarizations largely sampled the energy gap on the electron bands, while A_{1g} was more sensitive to the hole bands in the pnictides. Here we explore the form for the Raman vertices in more detail using local-density approximation (LDA).

The Raman vertices shown in Eq. (2) are directly computable from the one-electron band structure. We have performed full-potential linearized augmented plane wave (LAPW) calculations using the WIEN2K package and an experimental crystal structure, including the spin-orbit interaction. The doping is accounted for in the virtual-crystal approximation. The derivatives of the eigenstates were calculated numerically using a $31 \times 31 \times 31$ k-point mesh in the bct BZ. We neglect any momentum interplay between the Raman vertices and the superconducting gaps in the Tsuneto-Maki function and examine just the character of the Raman vertices on each band for each polarization geometry.[12] The calculated quantities are derived from evaluating Eq. (4) as

$$\chi_{\gamma,\gamma}^{sc} = \sum_{n,\mathbf{k}} \gamma_n^2(\mathbf{k}) \delta[\varepsilon_n(\mathbf{k})] - \frac{\left\{ \sum_{n,\mathbf{k}} \gamma_n(\mathbf{k}) \delta[\varepsilon_n(\mathbf{k})] \right\}^2}{\sum_{n,\mathbf{k}} \delta[\varepsilon_n(\mathbf{k})]}. \quad (5)$$

This can be simplified by writing $\gamma_n(\mathbf{k}) = \Delta\gamma_n(\mathbf{k}) + \bar{\gamma}_n$ with $\bar{\gamma}_n = \Sigma_{\mathbf{k}} \gamma_n(\mathbf{k}) \delta[\varepsilon_n(\mathbf{k})]/\Sigma_{\mathbf{k}} \delta[\varepsilon_n(\mathbf{k})]$ the average of the Raman vertex for band n over Fermi-surface sheet n. The response can be separated into an intraband piece, which is the only contribution for B_{1g} and B_{2g},

$$\chi_{intraband} = \sum_{n,\mathbf{k}} [\Delta\gamma_n(\mathbf{k})]^2 \delta[\varepsilon_n(\mathbf{k})], \quad (6)$$

and an interband contribution only appearing for A_{1g} channels $\Sigma_n N_n \bar{\gamma}_n^2 - (\Sigma_n N_n \bar{\gamma}_n)^2/\Sigma_n N_n$. The last part can be written as a band-dependent sum,

$$\chi_{interband} = \sum_n \frac{N_n}{N_t} \bar{\gamma}_n \sum_m N_m(\bar{\gamma}_n - \bar{\gamma}_m) = \sum_n \chi_{n,interband} \quad (7)$$

with $N_t = \Sigma_n N_n$ the total density of states (DOS). The results are shown in Table I and are defined as follows:

$$N_n = \sum_{\mathbf{k}} \delta[\varepsilon_n(\mathbf{k})],$$

$$\gamma_{n,\alpha\beta} = \sum_{\mathbf{k}} [\partial^2\varepsilon_n(\mathbf{k})/\partial k_\alpha\,\partial k_\beta]\delta[\varepsilon_n(\mathbf{k})],$$

$$\gamma_{n,\alpha\beta\gamma\delta} = \sum_{\mathbf{k}} [\partial^2\varepsilon_n(\mathbf{k})/\partial k_\alpha\,\partial k_\beta][\partial^2\varepsilon_n(\mathbf{k})/\partial k_\gamma\,\partial k_\delta]\delta[\varepsilon_n(\mathbf{k})],$$

such that the B_{1g} polarizations select $(\gamma_{n,xxxx} - \gamma_{n,xxyy})/2$, B_{2g} selects $\gamma_{n,xyxy}$. The unscreened intraband part for A_{1g} is given by $(\gamma_{n,xxxx} + \gamma_{n,xxyy})/2$, which is reduced with screening to $(\gamma_{n,xxxx} + \gamma_{n,xxyy})/2 - N_n\bar{\gamma}^2$.

The LDA results shown in Table I indicate that both B_{1g} and B_{2g} polarizations give vertices which are dominated by contributions from the electron FS, in agreement with the assessment of Ref. 6. Moreover we note that B_{1g} vertices are specifically large only on a single electron FS sheet, given by the outer FS pocket centered at M. For the A_{1g} contribution, while the unscreened Raman vertex $\gamma_{xxxx} + \gamma_{xxyy}$ has large contributions from the hole band $h1$ and electron band $e2$, backflow largely cancels the intraband contribution, leaving a substantial interband contribution deriving largely from these same bands. These results support the conjecture based on symmetry in Ref. 6 that the hole bands would be probed for A_{1g} configurations more so than for B_{1g} and B_{2g}.

The LDA results indicate that the A_{1g} interband portion involves also a strong contribution from scattering between the electron band $e2$ and the hole band $h1$, coming from different signs of the Raman vertices in the two bands. As discussed in Ref. 11 the divergence at twice the gap edge which may appear in crossed polarization orientations (such as $B_{1g,2g}$) is removed in single-band superconductors for A_{1g} symmetries due to the gauge-invariant backflow which screens uniform charge displacements over many unit cells. In multiband systems, such as the pnictides, the superconducting response for A_{1g} symmetries may be written as[11]

$$\chi^{scr}_{A_{1g}}(\Omega) = \sum_{n,\mathbf{k}} [\gamma_n(\mathbf{k}) - \bar{\gamma}(\Omega)]^2 \lambda_n(\mathbf{k},\Omega) \qquad (8)$$

with λ_n given by Eq. (3). The Tsuneto-Maki function λ_n possesses divergences when $\Omega = 2|\Delta_n(\mathbf{k})|$. $\bar{\gamma}(\Omega)$ is another way of representing the frequency-dependent backflow in the superconducting state for A_{1g} symmetries,

$$\bar{\gamma}(\Omega) = \sum_{n,\mathbf{k}} \gamma_n(\mathbf{k})\lambda_n(\mathbf{k},\Omega) / \sum_{n,\mathbf{k}} \lambda_n(\mathbf{k},\Omega). \qquad (9)$$

Each separate divergence occurring at the gap edge in each band in $\lambda_n(\mathbf{k},\Omega)$ weighs exactly those momentum points in $\gamma_n(\mathbf{k})$ for which the divergence occurs and via Eq. (8) the divergence is canceled. This holds for each divergence coming from each band n and therefore we conclude that no divergence may appear in A_{1g} symmetries for multiband systems. This conclusion holds only for Cooper-pair creation via light scattering but does not consider additional divergences coming from charge or spin collective modes.[13,14]

This predicted absence of an A_{1g} divergence is in general agreement in the observed data on the pnictides, where no clear 2Δ scattering peak is seen for A_{1g} scattering geometries. While sharp collective modes may appear due to the oscillation of pairing amplitudes in the different bands for

TABLE I. Values of the Raman vertices and related quantities including spin-orbit coupling around the hole ($h1,h2,h3$) and electron ($e1,e2$) Fermi surfaces, on a per cell basis, in Ry units (energy in Ry, distance in Bohr radii, momentum in inverse Bohr radii). Here $h1\cdots h3/e1\cdots e2$ denote the outermost$\cdots$innermost hole/electron barrel Fermi surface, centered at Γ/M in the Brillouin zone, as indicated in Fig. 2.

	$h1$	$h2$	$h3$	$e1$	$e2$
N_n	10.85	16.4	12.97	12.33	10.84
$(\gamma_{xx}+\gamma_{yy})/2$	−18.2	−9.9	−12.3	9.1	19.7
$\bar{\gamma}$	−1.7	−0.6	−1.0	0.74	1.8
$(\gamma_{xxxx}+\gamma_{xxyy})/2$	39.2	9.4	15.9	19.7	47.8
A_{1g} (intraband)	7.8	2.6	2.9	15.1	12.7
A_{1g} (interband)	28.6	3.6	7.7	8.6	38.9
B_{1g}	2.2	4.3	6.3	32.8	8.5
B_{2g} (averaged)	4.8	8.5	5.2	21.8	13.8

A_{1g} symmetries,[15] no clear indication of such a mode has been found. Similarly, although collective modes have been predicted to also occur in B_{2g} symmetries due to final-state excitons having orthogonal symmetry to the superconducting pair state,[16] it is still an open question whether these modes can be uncovered in the data.

The fact that in the experiment hardly any effect of superconductivity is observed in the B_{1g} polarization, while the calculations predict a noticeable coupling with the outer electronic FS, suggests that this coupling is not uniform, but is small wherever the gap is sizeable, and where the coupling is large the gap is small. In order to test this hypothesis, we have plotted the effective-mass asymmetry, appearing in B_{1g} polarizations as $|\partial^2\varepsilon_n(\mathbf{k})/\partial k_x^2 - \partial^2\varepsilon_n(\mathbf{k})/\partial k_y^2|$, in Fig. 2. We observe that, first, this difference is small on all FSs except the outer e-barrel, and, second, it is also small on the most of that FS as well, except on a small spot located at an angle varying from 10° to 15°, depending on k_z. As Fig. 2 shows, this is consistent with gap nodes or deep gap minima, forming elliptical loops on the outer electron FS centered around the $(\xi,\xi,0)$ points, where the Γ-M line intersects the electron pockets (indicated by the ellipse in Fig. 2). This can be compared with model calculations by Graser et al.[7] who found that the pairing interaction is strong in the Z plane ($k_z = \pi/c$) and weaker in the Γ plane. In their calculations
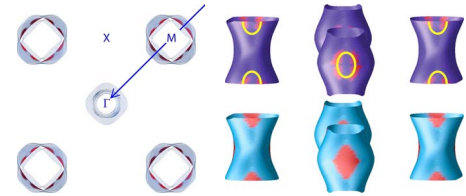

FIG. 2. (Color online) Left: Raman vertices for B_{1g} symmetry, evaluated around each Fermi-surface sheet projected onto the x-y plane. The Fermi surface sections are shaded dark (red) for maximal values of the B_{1g} vertex . Right top: the same, viewed along the M-Γ line, as shown by the arrow in the left panel; only the outer electron FS pockets are shown. The bright (gold) ellipses mark the area where the deep gap minima or nodes are expected. Right bottom: the same view but now the parts where the Fermi velocity is larger than 60% of its maximal value are shaded (red).

this led to a nodal loops similar to ours but located at the hole FS. One should be, however, careful, when making a quantitative, as opposed to qualitative comparison with these calculations because as discussed above, Graser *et al.* worked in an unfolded BZ where the folding-induced 3D dispersion was emulated through enhance k_z hopping parameters.

It is also consistent with the thermal-conductivity data[5] (collected on another 122 material), which indicate that there are gap nodes present in the system, yet the specific heat does not seem to be affected by them. These data have been interpreted in terms of ultraheavy hole bands that contribute at least 80% to the DOS and ultralight electron bands that dominate the transport. However, the former assumption seems a bit too strong to be realistic. Yet if in $BaFe_2(As,P)_2$ the gap structure resembles the one that we propose here for $Ba(Fe_{0.94}Co_{0.06})_2As_2$ so that the gap nodes exist only for a finite range of k_z, the rest of the electronic bands, fully gapped, add their contribution to the hole band and together provide 80% or more of the total specific heat. In fact, incidentally, the Fermi velocity is the largest close to the hot spots that we have identified as locations of gap nodes, in agreement with the idea that the transport is dominated by near-nodal parts of the FS (Fig. 2).

One can ask a question, why most of the Fermi surface, except for relatively small hot spots, shows such weak coupling in the B_{1g} channel. This is actually easy to address. Let us start with a simple model, a 2D parabolic electronic band. By symmetry, the principal axes of the corresponding elliptical FS are along (11) and $(1\bar{1})$. For the moment, we will use the center of this FS as the origin and the principal axes as coordinates. Then $\varepsilon_{1,2} = \mu_{1,2}\bar{k}_x^2 + \mu_{2,1}\bar{k}_y^2$. The Raman vertex in question appears like a B_{2g} vertex in this basis and is proportional to $\partial^2\varepsilon_n(\bar{k}_x, \bar{k}_y)/\partial\bar{k}_x\partial\bar{k}_y = 0$. Thus in this model this band does not couple in the B_{1g} channel at all.

However, this is not necessarily true if one takes into account the downfolding of the electron pockets in the crystallographic unit cell. After the downfolding the two FSs simply intersect. In our model, as well as in the real 11 and 1111 crystallography, they cross along the $\bar{k}_x = 0$ and $\bar{k}_y = 0$ directions, and, because they have different parities, there is no hybridization between them and the newly formed degeneracy is not lifted (although it would be lifted by the spin-orbit coupling). On the other hand, in the 122 symmetry the intersections occur at general points in the Brillouin zone so that no symmetry prevents them from hybridization thus forming an inner barrel and an outer barrel ($e1$ and $e2$) even

without the spin orbit. To gain more insight into this problem we introduce hybridization into our model and write the Hamiltonian near the anticrossing point as $H_{11} = \varepsilon_1(\bar{\mathbf{k}})$, $H_{22} = \varepsilon_2(\bar{\mathbf{k}})$, $H_{12} = H_{21} = V$, where V is a hybridization matrix element. The inverse masses of the resulting two bands are

$$\left| \frac{\partial^2 \varepsilon_\pm}{\partial \bar{k}_x \, \partial \bar{k}_y} \right| = \frac{8V^2|(\mu_1 - \mu_2)^2 \bar{k}_x \bar{k}_y|}{[(\mu_1 - \mu_2)^2(\bar{k}_x^2 - \bar{k}_y^2)^2 + 4V^2]^{3/2}}. \quad (10)$$

This is essentially an approximate expression of a delta function centered at $\bar{k}_x \pm \bar{k}_y = 0$ with the width V and strength $|\mu_1 - \mu_2|$. Thus in this simple model we have vanishing coupling everywhere except hot spots where the bands would cross if the As sublattice would not have a lower symmetry than the Fe one.

This simplified picture only qualitatively applies to Ba122. The bands there are not exactly parabolic, and, most importantly they cross not at the $\bar{k}_x, \bar{k}_y = 0$ lines, but at general points that can be considerably removed from these line, depending on k_z. Yet our model demonstrates qualitatively how the hot spots for this polarization appear on the FS, and why they are so small in size.

In summary, in this Rapid Communication, we have paired experimental data on the electronic Raman scattering in the superconducting state of $Ba(Fe_{0.94}Co_{0.06})_2As_2$ with the first-principles calculations of the effective-mass fluctuations. We found that a 2D TB model in the unfolded Brillouin zone is not sufficient to capture all the mass fluctuation. The reason is that because of the body-centered symmetry of the corresponding crystal structure downfolding the electron bands results in hybridizations and substantial band anticrossings, which in turns produces large-mass fluctuation in a small part of the Fermi surface. Our results suggest that closed nodal loops (rather than vertical or horizontal nodal lines) exist in this compound near the intersection of the outer electron Fermi surface with the Γ-M line. It is likely that the size and the very existence of these loops is doping dependent but this is beyond the scope of this Rapid Communication.

[1] T. Kondo *et al.*, Phys. Rev. Lett. **101**, 147003 (2008).

[2] H. Ding *et al.*, EPL **83**, 47001 (2008).

[3] K. Terashima *et al.*, Proc. Natl. Acad. Sci. U.S.A. **106**, 7330 (2009).

[4] D. Johnston, Adv. Phys. **59**, 803 (2010).

[5] Y. Matsuda (unpublished).

[6] B. Muschler *et al.*, Phys. Rev. B **80**, 180510(R) (2009).

[7] S. Graser *et al.*, Phys. Rev. B **81**, 214503 (2010).

[8] I. I. Mazin *et al.*, Phys. Rev. B **78**, 085104 (2008).

[9] T. P. Devereaux and R. Hackl, Rev. Mod. Phys. **79**, 175 (2007).

[10] M. Kang *et al.*, Phys. Rev. Lett. **77**, 4434 (1996).

[11] T. P. Devereaux *et al.*, Phys. Rev. B **54**, 12523 (1996).

[12] M. C. Krantz *et al.*, Phys. Rev. B **51**, 5949 (1995).

[13] A. V. Chubukov *et al.*, Phys. Rev. B **73**, 094512 (2006).

[14] M. V. Klein, Phys. Rev. B **82**, 014507 (2010).

[15] A. V. Chubukov *et al.*, Phys. Rev. B **79**, 220501 (2009).

[16] D. J. Scalapino and T. P. Devereaux, Phys. Rev. B **80**, 140512 (2009).